A spherical model with directional interactions: II. Dynamics and landscape properties

Christian Mayer[1,2]**, Francesco Sciortino**[1,2]**, Piero Tartaglia**[1,3] **and Emanuela Zaccarelli**[1,2]

[1] Dipartimento di Fisica, Università di Roma La Sapienza, Piazzale Aldo Moro 2, I-00185 Rome, Italy
[2] CNR-INFM-SOFT, Università di Roma La Sapienza, Piazzale Aldo Moro 2, I-00185 Rome, Italy
[3] CNR-INFM-SMC, Università di Roma La Sapienza, Piazzale Aldo Moro 2, I-00185 Rome, Italy

E-mail: emanuela.zaccarelli@phys.uniroma1.it

Abstract

We study a binary non-additive hard-sphere mixture with square well interactions only between dissimilar particles. An appropriate choice of the inter-particle potential parameters favors the formation of equilibrium structures with tetrahedral ordering (Zaccarelli *et al* 2007 *J. Chem. Phys.* **127** 174501). By performing extensive event-driven molecular dynamics simulations, we monitor the dynamics of the system, locating the iso-diffusivity lines in the phase diagram, and discuss their location with respect to the gas–liquid phase separation. We observe the formation of an ideal gel which continuously crosses towards an attractive glass upon increasing the density. Moreover, we evaluate the statistical properties of the potential energy landscape for this model. We find that the configurational entropy, for densities within the optimal network-forming region, is finite even in the ground state and obeys a logarithmic dependence on the energy.

(Some figures in this article are in colour only in the electronic version)

1. Introduction

Understanding dynamic arrest in a colloidal system is crucial for disparate technological applications, including the food industry [1] and biomaterials [2]. Development of basic science also requires a deeper understanding of the different routes and mechanisms leading to dynamic arrest (glasses and gels) [3–7].

Hard spheres (HS), representing the simplest colloidal model system, undergo an (ideal) glass transition at large densities [8, 9]. When short-ranged attraction complements the hard-core repulsion, the glass transition scenario becomes more complex, exhibiting two types of dynamic arrest mechanisms leading to both attractive and repulsive glasses, whose interplay shows anomalous dynamics (featuring sub-diffusive behavior for the mean-squared displacements and

logarithmic decays for the density autocorrelation functions) and glass–glass transitions. These features have been predicted by the mode coupling theory (MCT) [10–13] and confirmed under various aspects by numerous simulations [14–18] and experiments [19–21].

The situation is less clear at lower densities, where gel states may be formed under different routes [7]. Recent studies have shown that when a hard-core is complemented by an isotropic short-ranged attractive potential, the slowing down of the dynamics at low densities occurs as an arrested phase separation [22], interrupted by the intervening attractive glass line. Similar results are found for Lennard-Jones systems [23]. Therefore, homogeneously arrested states are only possible at high densities. The recent investigation of models with limited valence (*patchy* models) has shown that phase separation can be pushed to smaller and smaller

densities [24–31], accessing the formation of gels directly from the fluid phase (*equilibrium gels*). Patchy models are becoming increasingly important because of the recent progresses achieved in chemical synthesis [32–34] providing an unprecedented spectrum of colloidal molecules of various shape and functionality [35].

Recently, the analogy between colloidal gels/strong molecular glass-forming liquids and colloidal glasses/fragile molecular liquids has been put forward [36]. This analogy is based, among other things, on the Arrhenius dependence on temperature of the dynamical behavior exhibited by models of colloidal gels [37–40], typical of strong glass-formers [41]. Glasses driven by packing only show a super-Arrhenius behavior typical of fragile glass-formers. In the potential energy landscape (PEL) formalism [42], fragile liquids are described by a Gaussian density of states—the local minima of the PEL, named inherent structures (IS)—while this description breaks down at small temperature in strong glass-formers [43]. Simultaneously, the configurational entropy S_{conf}, defined as the logarithm of the number of IS with the same energy (degeneracy) does not extrapolate to zero at a finite temperature [37]. That suggests that there is no finite Kauzmann temperature [44, 41] in strong liquids.

Recently, it was proposed that strong and fragile behavior can also be differentiated by the intrinsic degeneracy of fully bonded disordered networks [37]. This study was based on the N_{max} model [45, 46] of network-forming liquids, which is also a model of colloids with fixed-valence. In this simple model, angular constraints in the bond formation are completely absent, while a many-body term in the Hamiltonian is used to limit the number of bonded neighbors. More recently, we have introduced [47] a spherical pair-wise additive model with directional interactions, which are realized by using a binary mixture of non-additive hard spheres. While large particles mimic the colloidal particles, small particles act as bonds between the large ones [48]. The interaction is attractive only between small and large particles and it is modeled via a short-range square well potential. To control the valence, the hard-core interaction between small particles is chosen significantly larger than their actual size. We have focused so far on a specific choice of the potential parameters, such that the maximum number of bonds a large particle can form is limited to four. In this way, at low temperatures where most of the bonds are formed, the system self-organizes into a tetrahedral network. Following [39, 49], the region where the average density of the system allows for the establishment at low T of a fully connected network (i.e. the region of densities where the ground state of the system can be reached) is named optimal network-forming density region. This region is limited at low densities by the gas–liquid phase separation. At high density, packing constraints do not allow the formation of a shell of nearest neighbors with the right orientation requested for full bonding [39, 49], preventing the establishment of a tetrahedral and fully bonded network.

In this article we complement the previous investigation of the static properties with results for the particle dynamics, which allow us to locate the arrest transition line with respect to the equilibrium phase diagram. We find the presence of

ideal gels in the optimal network-forming region, as well as attractive and repulsive glass lines at larger densities. The present results confirm the behavior previously found for the N_{max} model, but with some important differences. First, frustration becomes important at large packing fractions, hindering the possibility of satisfying simultaneously all possible bonds. Secondly, a clear structural tetrahedral ordering is now present (induced by the effective constraints realized by the small particles). Finally, the bonding constraints are capable to efficiently localize the particles between the attractive bonds, generating the typical signatures of an attractive glass.

Since the inter-particle potential is pair-wise additive and spherical symmetric, this simple model is suitable for studying the statistical properties of the potential energy landscape (PEL). In addition, the ground state is known *a priori*. Thanks to a straightforward generalization to binary mixtures of the approach followed for the N_{max} model, we evaluate the properties of the PEL in a formally exact way and provide an estimate for the configurational entropy of the fully bonded network.

The article is organized as follows. In section 2 we present the studied model. We discuss results from MD simulations, focusing on the mean-squared displacement (MSD) and long-time self-diffusion coefficient D in section 3. The method we use to calculate the configurational entropy is briefly reviewed in section 4.1 and the results obtained are discussed in section 4.2. Finally we draw our conclusions in section 5.

2. Model system

Following [47], we consider a binary mixture of N_1 hard spheres (*particles*) with diameter σ_{11} and N_2 smaller particles (*floating bonds*) with a hard-sphere diameter σ_{22}. The interaction between the two species is given by a hard-core accompanied by a square well (SW) attraction,

$$V_{12}(r) = \begin{cases} \infty & r < \sigma_{12} \\ -u_0 & \sigma_{12} < r < \sigma_{12} + \delta \\ 0 & r > \sigma_{12} + \delta. \end{cases} \quad (1)$$

The parameters are chosen in order to ensure that the small particles act as floating bonds connecting two large colloids only. The small–small hard-sphere diameter is selected in such a way that every large sphere can accommodate at most four small particles in a tetrahedral arrangement around itself. This is possible thanks to the choice of $\sigma_{22} = 0.8\sigma_{11}$, and of a non-additive cross-interaction with $\sigma_{12} = 0.55\sigma_{11}$. Additionally, we use $\delta = 0.03\sigma_{12}$. Therefore, the non-additivity parameter $\Delta = 2\sigma_{12}/(\sigma_{11} + \sigma_{22}) - 1 = -0.389$. We consider two large particles to be bonded when they are bound to the same floating bond. Due to the square well form of the potential, bonds can be unambiguously identified when two particles are found within the attractive well distance. The model is built in such a way that its ground state energy is known and corresponds to the fully bonded network with four bonds per particle. We can then define the bond probability p_b as the ratio between the number of formed bonds and the maximum number of bonds.
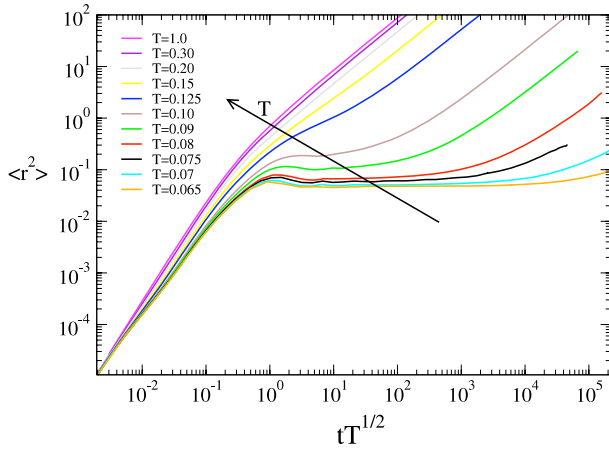
Figure 1. MSD along the isochore $\phi = 0.25$, within the optimal network-forming region, at various studied T.

Figure 2. MSD for $T = 0.10$ at various studied ϕ. The horizontal dashed lines represent the (approximate) hard-sphere and attractive glass plateaux.

Packing fraction is defined as $\phi = \pi N_1 (\sigma_{11}/L)^3/6$, i.e. as the fraction of volume occupied only by the large particles.

The static properties of this system have been studied in detail [47]. In the first article of this series it has been shown, that a fully bonded tetrahedral network develops for low temperatures in the optimal density region, i.e. $0.23 < \phi < 0.4$, which is delimited at low ϕ by phase separation and at large ϕ by the increasing effect of packing which tends to hinder the formation of a perfect network [39, 49]. Here we complement this study with an investigation of the dynamics of the system, as well as of the energy landscape properties.

3. Dynamics

3.1. MD simulations

We carried out molecular dynamics (MD) simulations with $N_1 = 1000$ large particles and $N_2 = 2000$ floating bonds (with the same mass) for several state points in the packing fraction/temperature (ϕ, T) diagram, as already reported in [47]. After equilibration is achieved (in the NVT ensemble), the dynamics of the system is monitored, performing simulations in the NVE ensemble. Units of length, mass and energy are the large particle diameter σ_{11}, the particle mass m, and the square well depth u_0, respectively. Temperature T is measured in units of energy, with $k_B = 1$. Time is measured in units of $\sigma_{11}(m/u_o)^{1/2}$. Our analysis for the dynamics focuses on the large particles only. We calculate the mean-squared displacement (MSD) $\langle r^2(t) \rangle$ and extract the self-diffusion coefficient $D \equiv \lim_{t \to \infty} \langle r^2(t) \rangle /6t$ of the particles. We use the values of D in the ϕ–T plane, to draw iso-diffusivity lines, i.e. lines along which D—normalized by the bare diffusion coefficient $D_0 \equiv \sigma_{11}\sqrt{T/m}$—is constant. These lines are precursors, in a shape-invariant way [50, 16, 51–53], of the (ideal) arrest line, defined as the line for which D vanishes.

3.2. Mean-squared displacements and localization lengths

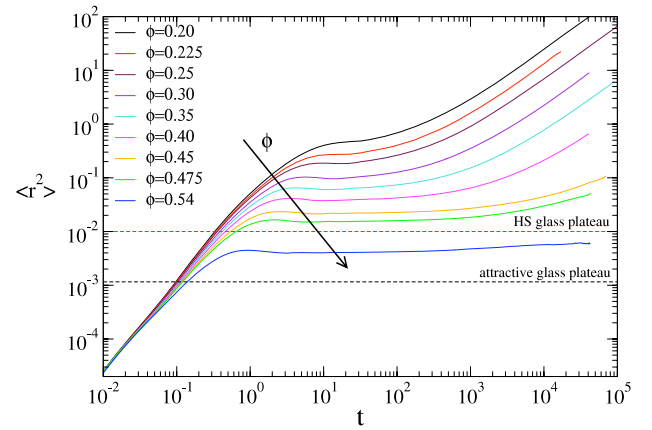We start by reporting the MSD at fixed packing fraction $\phi = 0.25$, within the optimal network-forming region [47], upon lowering T in figure 1. Data are shown as a function of $tT^{1/2}$ to take into account the thermal dependence of the microscopic time. It appears immediately that, with decreasing T the system becomes slower and slower and a clear long-time (but still transient) plateau emerges for $T \lesssim 0.10$, which becomes longer and longer with decreasing T. The height of this plateau provides a measure of the squared localization length l_0 of the cage in which particles are trapped. Such height decreases upon decreasing T until, at the lowest studied points ($T \lesssim 0.075$), the system arrests (within the explored time window t_{MAX}), since $\langle r^2(t_{MAX}) \rangle \ll \sigma_{11}^2$. The plateau height seems to saturate at a localization length $l_0 \sim 0.25\sigma_{11}$. This saturation takes place because the system, at this finite T, has already developed an almost fully bonded network ($p_b \sim 0.95$) and no significant structural changes are expected on further cooling. At very long times, the system is still able to escape the plateau, eventually recovering a (very slow) diffusive behavior, due to the long, but still finite at finite T, lifetime of the bonds.

It is interesting to notice also that the MSD displays two slowing-down mechanisms. In addition to the long-time plateau discussed above, a second slowing down takes place just after the microscopic time, when particles have traveled a squared distance $\langle r^2 \rangle \sim 3 \times 10^{-4}$, which is compatible with the squared (half-)bond distance δ^2. Such a slowing down due to the attractive bonds has been observed in simulations of other gel-forming systems [54, 55].

In figure 2 we plot the MSD versus time at fixed $T = 0.10$ for several studied ϕ. We observe the development of a clear plateau, which becomes longer and longer and, most importantly, which decreases in height by several orders of magnitude with increasing ϕ. This decrease appears to be continuous: a flat plateau is observed at all studied ϕ, without the intervening of any sub-diffusive regime at intermediate times. The cage size varies from large values typical of 'gel' states down to well below the HS expected glass value, i.e. $l_0^{HS} \sim 0.10\sigma_{11}$. This behavior is different from that observed for the N_{max} model [38], where a competition between the two mechanisms, gel and repulsive glass, gives rise to a region of sub-diffusive behavior in ϕ, instead of a
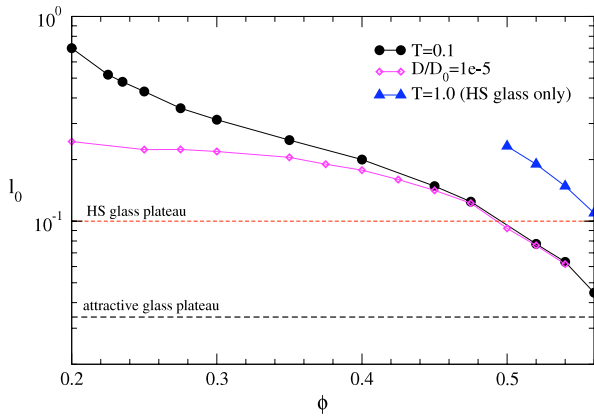
Figure 3. Localization length l_0 as a function of ϕ along the low-T isotherm $T = 0.10$, along the high T isotherm $T = 1.00$ and along the iso-diffusivity line for which $D/D_0 = 10^{-5}$. The latter provides an estimate of the cage size within the arrested states (gels and attractive glasses) for various ϕ.

Figure 4. MSD for $\phi = 0.54$ at various studied T. Note the reentrant behavior in T, so that dynamics is fastest around $T = 0.75$. The dashed line is a power-law fit to the $T = 0.20$ curve, signaling sub-diffusive behavior for about three decades in time with an exponent ≈ 0.15.

transient plateau, for a similar attraction strength. On the other hand, in the $N_{\max}$ case, we never observed a decrease of l_0 below l_0^{HS}, oppositely to what found here for comparable low-T state points. Hence, it appears that the explicit presence of floating bonds favors the observation of the typical signatures of an attractive glass.

To investigate the approach to the attractive glass, we plot in figure 3 the localization length versus ϕ for $T = 0.10$. For comparison we also report l_0 at large T (namely $T = 1.0$), for which the system tends to approach the HS glass transition at high ϕ. For $T = 0.10$, l_0 decreases monotonically until, for $\phi > 0.50$, it falls well below the HS glass typical value. Since there is a large residual T dependence for the low/intermediate densities at this T, we also estimate l_0 along the slowest iso-diffusivity curve (see below) for which $D/D_0 = 10^{-5}$. The dependence of l_0 along this curve, also reported in figure 3, shows that in the optimal network-forming region, once the system has approached the ground state energy, the size of the cage is roughly constant within our numerical error. At larger ϕ, the size decreases substantially and l_0 reaches values very close to the typical attractive glass value, i.e. squared total bond distance $(2\delta)^2 \sim 0.001$. Since the system is not allowed to restructure any further and dynamics is already extremely slow, this line can be viewed as an estimate of the cage size within the arrested state. It is interesting to notice the existence of a roughly constant value for the gel states, $l_0 \sim 0.2\sigma_{11}$, which is compatible with the distance between two particles mediated by the floating bonds, followed by a decrease in the high-density region. We could interpret this finding as a signature of a gel-to-attractive-glass transition as ϕ increases. Indeed, while in the gel state rattling is possible within the full total distance between two particles, allowing floppy rearrangements of the particles, with increasing ϕ, rattling becomes more and more localized within the attractive well only. It would be interesting to investigate a constant low-T path, starting actually from a gel configuration, to investigate if the crossover is continuous. In this respect, the present model is the first example which offers both perfect network equilibrium gel states as well
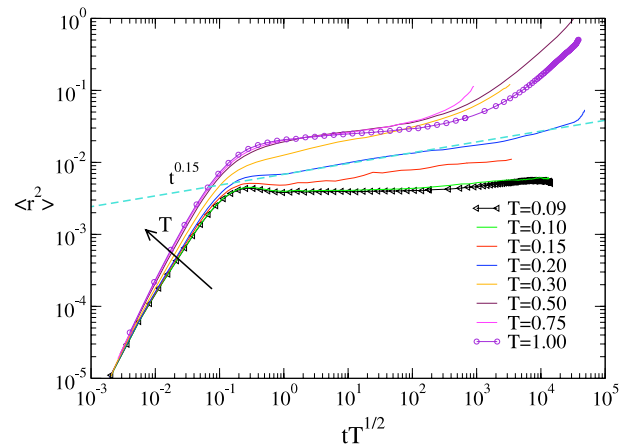
as glasses of both repulsive and attractive nature. For this reason, a comparison of the density correlators plateau and arrest mechanisms with MCT predictions will be important to elucidate further the nature of the gel/attractive glass transition, and it will be the subject of our future studies.

Finally, to show the interplay between repulsive and attractive glasses we report the MSD at large density, i.e. $\phi = 0.54$ in figure 4. Although the length of the simulation runs is not sufficient to recover a long-time diffusive behavior at all T, we detect all the typical features of a standard SW model. First, at high T, a reentrant behavior of the dynamics is observed as found in simulations of simple spherical models [50, 16, 15] and in experiments on colloidal spheres with attractive depletion interactions [21, 56], in agreement with MCT predictions [10, 12]. Then, a sub-diffusive behavior appears, again in agreement with simulations [16] and MCT [57], which was attributed to the competition between the attractive and the repulsive glass. We notice that the attractive-glass-like plateau observed here is among the most stable ever observed in simulations [58, 59]. We may attribute this behavior to the effective reduction of hopping mechanism for the present model. Indeed, the floating bonds are able to constrain quite effectively the particles within the bonds and hence act as a stabilization mechanism for bonds, without the need to invoke rigidity and angular constraints. This is also due to the fact that the reduced valence shifts the cross-over between the two glasses at lower T compared to the isotropic case.

3.3. Self-diffusion coefficient and iso-diffusivity lines

We report in figure 5 the behavior of the self-diffusion coefficient for the state points that recover long-time diffusivity in an Arrhenius plot. We observe a robust Arrhenius dependence of D with T at all studied ϕ, with an activation energy which is roughly 1.8, a value amounting to about four times the value of the activation energy for the potential
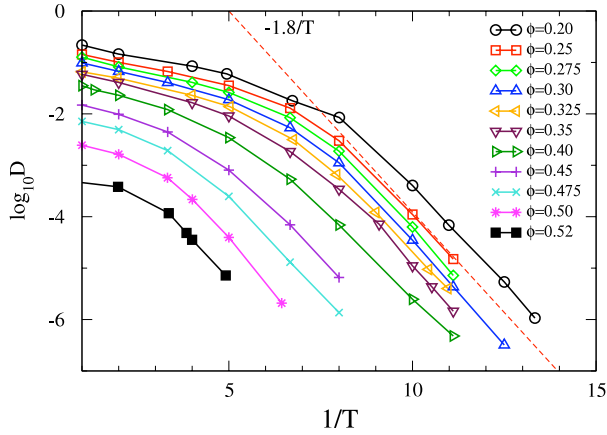
Figure 5. Arrhenius plot of the diffusion coefficient along the studied isochores. The dashed line indicates that the activation energy is roughly 1.8.
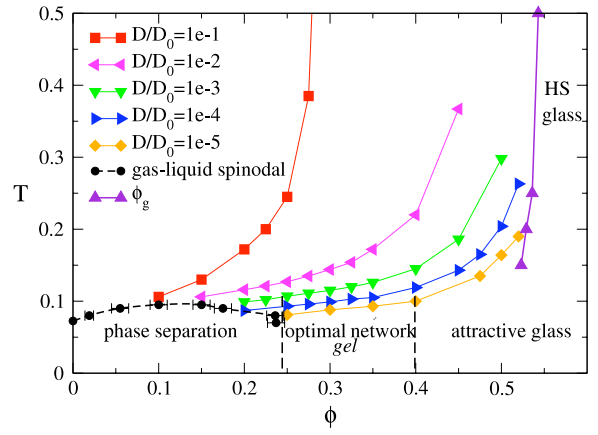

Figure 7. Phase diagram, partially redrawn from [47], with the addition of the iso-diffusivity lines, covering 4 orders of magnitude in D/D_0, as well as the glass line ϕ_g extrapolated from power-law fits.
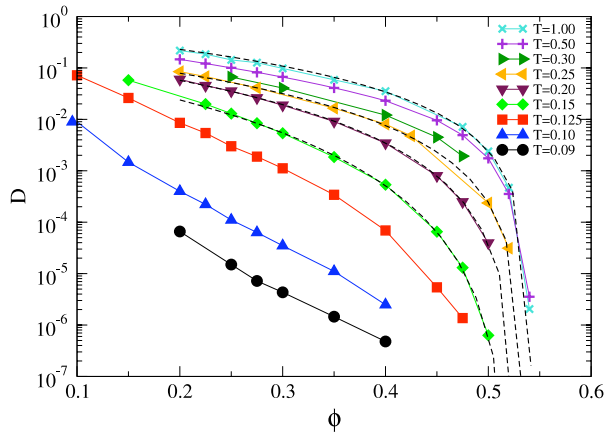
Table 1. Summary of fit parameters for the power-law dependence of D with ϕ.

T	ϕ_g	γ
1.00	0.542	2.17
0.50	0.543	2.18
0.25	0.536	2.59
0.20	0.529	3.00
0.15	0.523	3.98

Figure 6. Diffusion coefficient dependence on ϕ for various studied isotherms. At high T, data are compatible with power-law behavior. Dashed lines are power-law fits, corresponding to the parameters reported in table 1.

energy [47], which also displays an Arrhenius dependence at low T in the optimal network region. For large ϕ, it becomes more and more difficult to estimate unambiguously the functional form of the T dependence of D (due to the computational difficulty to probe slow states at low T). Still, data seem to be compatible with an Arrhenius law. Hence, the T dependence of the dynamics appears to be of strong character in the fully investigated dynamical window, covering both ideal gel and attractive glass states.

Turning to examine the density dependence of D, which is reported in figure 6, we find that a power-law fit, $D \sim (\phi_g - \phi)^\gamma$, is able to well describe the high-T data down to $T = 0.15$. The parameters of such fits are reported in table 1. The systematic increase of the exponent γ suggests that the system becomes close to a higher order MCT singularity. The extrapolated ϕ_g values are also reported in the phase diagram of figure 7. For the lowest studied T, it appears that the data are still too far from the transition to establish whether a power-law dependence still holds. Hence, we cannot provide an estimate of ϕ_g, due the lack a clear diffusive regime in the MSD.

Finally, we report the evolution of the iso-diffusivity lines covering 4 orders of magnitude in D/D_0, where we have taken into account the trivial effect of temperature in the slowing down of the dynamics. The iso-diffusivity lines behave very similarly to those observed for other low-coordinated models [38, 39, 49, 60], with a horizontal slope at low ϕ turning rapidly into a vertical slope at high ϕ. This indicates that two arrest mechanisms are at hand: at high ϕ, excluded-volume caging occurs, which is almost T independent and caused by the nearby HS glass transition; at lower ϕ bonding essentially controls the dynamics, resulting in iso-diffusivity lines that become more and more parallel to the ϕ-axis. Here, an equilibrium network forms at low–intermediate ϕ arresting at lower and lower T into a gel state. The definition of the gel transition is intrinsically related to the bond lifetime definition and hence, technically, the ideal gel state (when the lifetime of the bonds becomes strictly infinite) is located at $T = 0$. Above the network-forming optimal region, the gel turns continuously into an attractive glass state. We find no evidence of competition or anomalous dynamics between these two states. On the other hand, we are not able to investigate in details, due to the extremely slow dynamics involved, the interplay between the two arrest (T-dominated and ϕ-dominated) lines. We aim to perform a comparison of the density autocorrelations functions, and the relative non-ergodicity parameters, calculated from simulations with the solutions of MCT equations in the future, to be able to shed more light on the interplay between the different arrested states.

4. Landscape properties

4.1. Evaluation of the configurational entropy

The potential energy landscape $U(\mathbf{r}^N)$ is a surface in the high-dimensional space of the coordinates of the N particles in the system. Employing the formalism introduced by Stillinger and Weber, we can split the configuration space into different local basins of attraction (called inherent structures, IS) [42]. The configurational entropy S_{conf} is defined as the logarithm of the number of IS with the same energy (degeneracy). The basic concept consists of splitting the total entropy into a vibrational part, corresponding to the motions of the particles within the basin of each IS, and a configurational part, which accounts for the distribution of the minima [61, 62].

In most systems the evaluation of the vibrational entropy requires some approximations. However, for systems interacting via step-like potentials as in the present case, an exact evaluation of the vibrational contribution is possible [37, 63, 64]. Indeed, in these systems, every IS is uniquely identified by a realization of the bonding pattern. In this way, no minimization is required to identify the IS.

Within the framework developed by Frenkel and Ladd [65], the excess vibrational entropy can be calculated starting from a reference Einstein crystal with a known free energy. For that purpose, the system Hamiltonian H_0 is complemented by a harmonic term of the form $H_\lambda = \lambda \sum_{i=1}^N (\mathbf{r}_i - \mathbf{r}_i^0)^2$, where $\mathbf{r}^0 = (\mathbf{r}_1^0, \ldots, \mathbf{r}_N^0)$ are the coordinates of the unperturbed system. In this way, the excess vibrational entropy $S_{\text{vib}}^{\text{ex}}$ for a system with number density $\rho = N/V$ is given by [63],

$$\frac{S_{\text{vib}}^{\text{ex}}}{N k_b} = \frac{3}{2} \ln \left(\frac{\pi k_B}{\lambda_{\text{max}}} \right) - 1 + \ln \rho$$
$$+ \beta \int_{-\infty}^{\ln \lambda_{\text{max}}} \lambda \left\langle \frac{1}{N} \sum_{i=1}^N (\mathbf{r}_i - \mathbf{r}_i^0)^2 \right\rangle_\lambda \, \mathrm{d} \ln \lambda$$
$$+ x_1 \ln(x_1) + x_2 \ln(x_2) \qquad (2)$$

where λ_{max} is the maximum coupling considered in the study, which has to be sufficiently large to satisfy the condition $\lambda_{\text{max}} \langle \sum_{i=1}^N (\mathbf{r}_i - \mathbf{r}_i^0)^2 \rangle_{\lambda_{\text{max}}} = 3N k_B T/2$, i.e., to recover the limit of N harmonic oscillators. The latter term arises from the mixing contribution to the total entropy, where $x_i = N_i/N$ ($i = 1, 2$) respectively.

To evaluate $S_{\text{vib}}^{\text{ex}}$ from equation (2), we perform Monte Carlo simulations, for the same system size used in the MD simulations, with the constraint that the bonding pattern is preserved. To evaluate the integral over λ, we have used 20 values of λ, ranging from 0 to λ_{max} spaced on a logarithmic scale [63]. The average displacement for the perturbed system are calculated performing several runs at each fixed value of λ.

In addition, we calculate the total entropy of the system for a given density and temperature by means of thermodynamic integration. To this aim, we evaluate numerically the equation of state for our non-additive hard-sphere mixture (i.e. the $T \to \infty$ limit of our model, equation (1)) to be used as reference system. To evaluate the excess free energy of the non-additive hard-sphere mixture we integrate,

$$\frac{\beta F_{\text{HS}}^{\text{ex}}}{N} = \int_0^\rho \frac{\beta P_{\text{HS}}^{\text{ex}}}{\rho'^2} \, \mathrm{d}\rho'. \qquad (3)$$

Table 2. Summary of the fit parameters used to describe vibrational and configurational entropy.

ϕ_1	γ_{vib}	$S_{\text{vib}}^{\text{ex}}(E_{\text{gs}})/N$	γ_{conf}	$S_{\text{conf}}(E_{\text{gs}})/N$	B	E_a
0.25	8.13	−9.20	0.862	0.383	3.0×10^4	0.44
0.35	6.27	−9.07	1.32	0.455	1.7×10^4	0.46
0.40	5.30	−9.19	1.51	0.453	1.1×10^4	0.45

In order to minimize the numerical error, we subtract the first virial correction to the ideal gas pressure and integrate its contribution analytically [66]. The virial coefficient for hard-sphere binary mixtures is:

$$B_2 = \tfrac{2}{3} x_1^2 \pi \sigma_1^3 + \tfrac{2}{3} x_2^2 \pi \sigma_2^3 + \tfrac{4}{3} x_1 x_2 \pi \sigma_{12}^3. \qquad (4)$$

The temperature dependence of the excess part of the total entropy for the floating bond model can thus be calculated as,

$$S_{\text{tot}}^{\text{ex}}(T) = S_{\text{HS}}^{\text{ex}} + \int_\infty^T \left(\frac{\partial E}{\partial T'} \right)_V \frac{\mathrm{d}T'}{T}, \qquad (5)$$

where $S_{\text{HS}}^{\text{ex}}$ is calculated numerically from equation (3) for the reference non-additive hard-sphere mixture. Due to the long equilibration times required, the S^{ex} at very small T has been estimated extrapolating using the Arrhenius fits, the low T dependence of E as reported in [47]. Indeed, in the optimal network region, the potential energy can be described as

$$E - E_{\text{gs}} = B \exp(-E_a/T), \qquad (6)$$

where E_{gs} is the energy of the fully bonded ground state and E_a is the corresponding activation energy. The best fit parameters are reported in table 2.

The configurational entropy S_{conf} is calculated as the difference between the total and the vibrational entropy:

$$S_{\text{conf}} = S_{\text{tot}} - S_{\text{vib}}, \qquad (7)$$

so that finally we obtain,

$$\frac{S_{\text{conf}}}{N k_B} = \frac{S_{\text{tot}}^{\text{ex}} - S_{\text{vib}}^{\text{ex}}}{N k_B}. \qquad (8)$$

4.2. Results: vibrational and configurational entropy

We start by evaluating the excess vibrational entropy $S_{\text{vib}}^{\text{ex}}$ of the system on the basis of equation (2). Results for three different packing fractions, all within the optimal network region, are shown in figure 8. In agreement with previous results [67, 68, 63], we find that the excess vibrational entropy exhibits a linear dependence on the potential energy of the system (figure 8—right). We describe this functional behavior by a fit of the form:

$$S_{\text{vib}}^{\text{ex}}(E) = S_{\text{vib}}^{\text{ex}}(E_{\text{gs}}) + \gamma_{\text{vib}}(E - E_{\text{gs}}). \qquad (9)$$

Using the Arrhenius dependence of $E(T)$ (equation (6)), we are also able to describe the T dependence of $S_{\text{vib}}^{\text{ex}}$, as shown in figure 8—left.

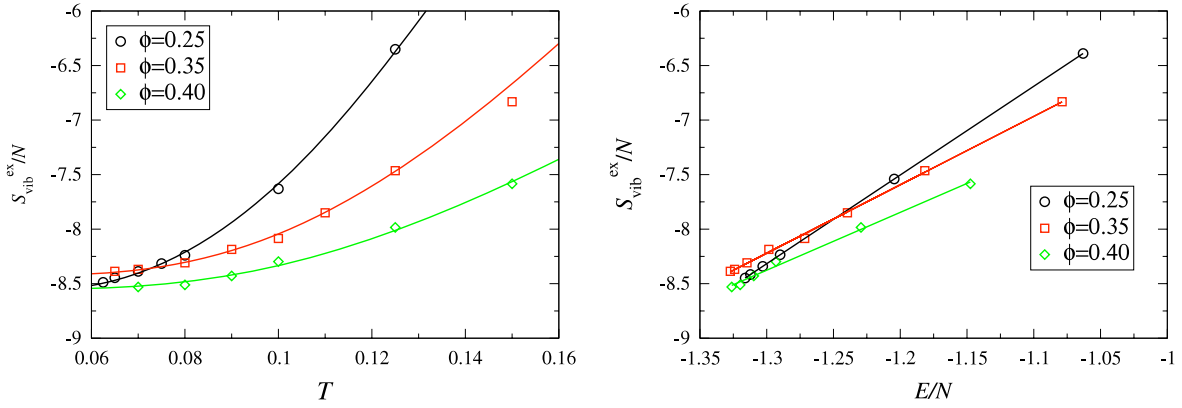In figure 9, the excess total entropy of the system, estimated from equation (5), is reported. We rely on the

Figure 8. Vibrational entropy evaluated using equation (2) for $\phi = 0.25, 0.35, 0.40$. Entropy as a function of temperature (left), as a function of energy (right). The solid lines correspond to the fits according to equation (9) and their reparametrization using the Arrhenius law for $E(T)$, equation (6).

Arrhenius behavior of the system in this optimal network-forming region to extrapolate the simulation data down to very low temperatures, below $T \lesssim 0.07$. We notice that, for such low T, the data points are already approaching a plateau, since we are very close to the ground state ($p_b > 0.95$ [47]), so that we can reliably extrapolate S_{tot}^{ex} to its $T \rightarrow 0$ value.

Following the derivation by Moreno *et al* [63], we write

$$\frac{\partial(S_{conf} + S_{vib})}{\partial(E - E_{gs})} = \frac{1}{T}. \tag{10}$$

Making use of equation (6), we obtain

$$\frac{1}{T} = -\frac{\ln[(E - E_{gs})/B]}{E_a}. \tag{11}$$

By describing the vibrational entropy by the fit of equation (9), we get the expression

$$\frac{\partial S_{conf}}{\partial(E - E_{gs})} = -\gamma_{vib} - \frac{\ln[(E - E_{gs})/B]}{E_a}, \tag{12}$$

which we integrate to arrive at the final result

$$S_{conf}(E) = S_{conf}(E_{gs}) - \frac{E - E_{gs}}{E_a} \ln[2(E - E_{gs})] + \gamma_{conf}(E - E_{gs}), \tag{13}$$

where we have defined

$$\gamma_{conf} = \frac{1}{E_a} - \gamma_{vib} + \frac{\ln(2B)}{E_a}. \tag{14}$$

Our raw data for S_{conf}, reported in figure 10 (as a function of T and E, respectively left and right panels) obtained directly from equation (8) are very well described by this functional form (equation (13)). The logarithmic dependence of $S_{conf}(E)$ has been interpreted as a distinct signature of the landscape properties of strong liquids, in contrast to the Gaussian dependence observed for fragile ones, and has been attributed to the number of distinct ways in which $(E - E_{gs})N$ bonds can be broken among N particles [37]. Hence, equation (13) can be used to obtain a reliable estimate for the configurational entropy for $T \rightarrow 0$. It is evident from figure 10
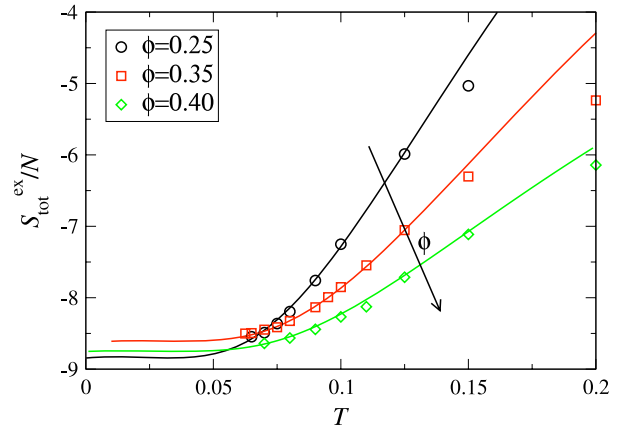

Figure 9. Excess total entropy as a function of temperature. The dashed lines show the extrapolation using the Arrhenius behavior of the energy, equation (6).

that the configurational entropy saturates to a finite value at low T, so that $S_{conf} > 0$ at zero temperature. This is caused by the degeneracy of the ground state, due to the fact that there are many realizations of the fully bonded network.

In table 2, a summary of the fit parameters used to describe the vibrational and configurational entropies is reported. We notice an increase of S_{conf} with ϕ, followed by a roughly constant value, in agreement with results obtained for the N_{max} model [63]. For a proper comparison, it is best to normalize the entropy by the number of large particles (i.e. by the number of nodes in the tetrahedral network). This corresponds to multiply by three (the ratio N/N_1) the values of S_{conf} in figure 10. As compared to the values observed for the 4-coordinated N_{max} model (network entropy of about 2) the present values are smaller, and we attribute this smaller value to the fact that the present model is able to effectively constrain the particles within a small bond angle, while in the N_{max} model any angular constraint is absent. Hence, the degree of degeneracy of the fully connected network obtained in the present model is, as expected, smaller.

In order to make a connection between the structural and dynamical data, we have also checked the validity of the
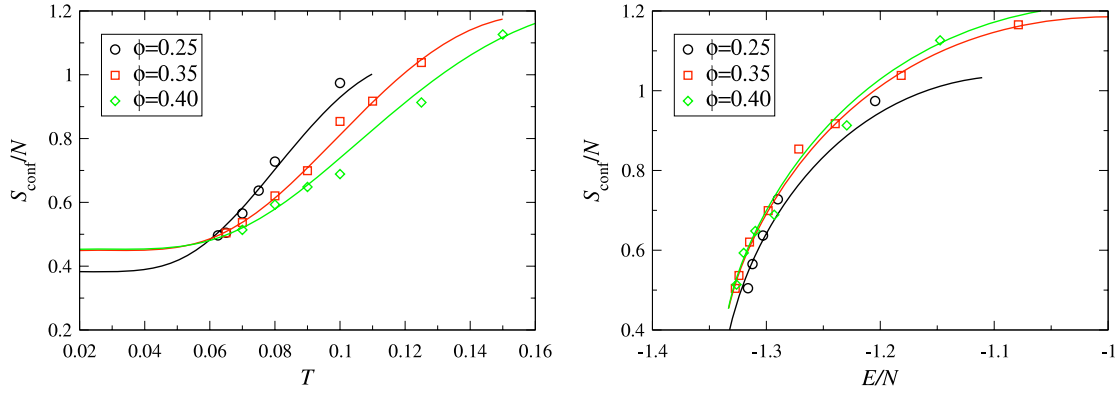
Figure 10. Configurational entropy calculated as the difference of total and vibrational entropy, equation (8). Entropy as a function of temperature (left) and as a function of energy (right). The solid lines correspond to fits according to equation (13) and their reparametrization using the Arrhenius law for $E(T)$, equation (6).

Adam–Gibbs relation [69] in our model. We find (not shown) that, indeed, the logarithm of the diffusion coefficient as a function of $(T S_{\text{conf}})^{-1}$ scales linearly.

　　One additional comment is devoted to the behavior of the landscape properties for $\phi > 0.40$. In this region, the system for $\phi > 0.40$ becomes increasingly frustrated and does not approach any longer a fully bonded network, but only a disordered network with more and more defects. Hence, the system reaches a (ill-defined) ground state energy, larger than the fully bonded one. Given that we cannot rely on the validity of the Arrhenius law for the approach to the ground state, we cannot provide a satisfactory estimate of S_{conf}. However, we notice that $S_{\text{vib}}^{\text{ex}}$ clearly deviates from the linear E dependence at low E, at odds with standard behavior of both strong and fragile glass-formers. The PEL properties in this region will be the subject of future investigations.

　　As a first step toward better interpreting the origin of the residual configurational entropy in the fully bonded state (which we tentatively associate with the disorder in the topology of the network), we evaluate the size distribution of primitive rings in the network, when the system has almost approached its ground state energy. We employ the definition and algorithm given in [70]. By this definition, a primitive ring is a ring that cannot be decomposed into two smaller rings. In figure 11, we report the number of rings n_{r}, normalized by the number of particles N_1, as a function of the size of the rings s_{ring} detected at three packing fractions and at $T = 0.08$, i.e. a sufficiently low T such that the system has formed an almost fully bonded network. The size of rings refers to the number of particles only, without counting the floating bonds. As can be seen from figure 11, the minimum number of particles in a ring is three, meaning that a ring consists of at least 6 hard spheres (particles and floating bonds). Moreover, a size of twelve is the maximum that we can detect within our simulation box, without counting periodic replicas of the rings.

　　We notice that for low ϕ, the number of rings is smaller, and also that the maximum of the distribution is found for $s_{\text{ring}} \simeq 6$, a number compatible with a diamond coordination and with the tetrahedral ordering observed in the static structure factors [47]. However, upon increasing ϕ for low T, this maximum shifts toward larger sizes and larger rings
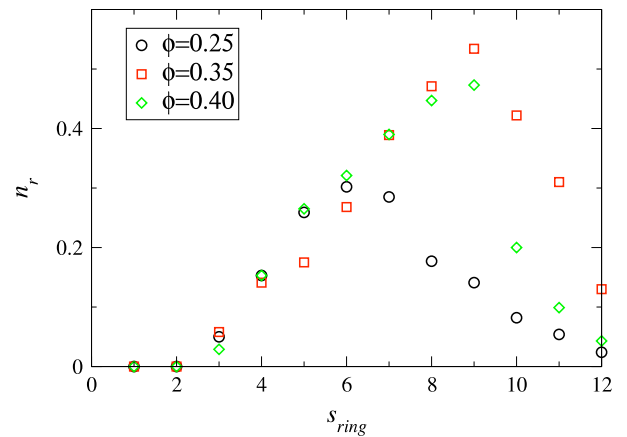

Figure 11. Ring size distribution n_{r} vs size of the rings s_{ring} for $T = 0.08$ for $\phi = 0.25, 0.35, 0.40$. The number of rings n_{r} is normalized by the number of large spheres N_1.

become more frequent. The distributions for $\phi = 0.35$ and 0.40 are very similar, as are the respective (extrapolated) configurational entropies.

5. Conclusions

In this work we have reported on the dynamic and landscape properties of a simple non-additive mixture, which although based on spherical interactions is able to reproduce the results for a network-forming liquid with directional interactions. Indeed, a very similar model designed to mimic silica has been recently discussed [71]. Our interest for this model lies in the context of similar patchy models for colloidal systems. In particular, we have shown that the dynamical properties are very similar to those of other 4-coordinated systems, which have been studied recently, i.e. the N_{max} model [38], a model for DNA-functionalized particles [60] and also primitive models for water [39] and silica [49]. Interestingly, a recent work has pointed out the similarity of the phase diagram of these systems, and its interplay with the iso-diffusivity lines, with respect to that of commonly employed models for

molecular liquids, such as SPC/E and ST2 for water and BKS for silica [36].

　　In the present study, we have shown that, within the optimal network-forming region, the dynamics slows down in an Arrhenius way, pointing to the formation of *ideal equilibrium gels* [7, 26]. Upon increasing ϕ, the system becomes more and more frustrated, due to packing. In the T-window where we are able to calculate reliable estimates for the self-diffusion coefficient, we do not see a deviation from Arrhenius law. In addition, we also observe a slowing down associated to the hard-core only at large ϕ, compatible with a power-law behavior. While the present study is not sufficient to resolve the complicated interplay between bonding and caging in this spherical but patchy model (but see a related recent work for simple square well interactions [59]), it offers the first evidence of a system encompassing both (ideal) gel and attractive glass states, as well as repulsive glasses. The gel can be discriminated from the attractive glass from the value of the localization length. Indeed, the length in the MSD remains always well above the typical glass value in the optimal network region. For larger ϕ the system seems to cross continuously to an attractive glass state, which is characterized by a very long and flat plateau in the MSD and by a very small localization length.

　　Another interesting feature of the present model is that it offers the possibility to evaluate the statistical properties of the landscape in a formally exact way. Simply generalizing previous calculations to binary mixtures, we have provided estimates for the configurational entropy within the optimum network-forming region and compared them with those for the N_{max} model. The presence of directional interactions diminishes the value of the S_{conf} for the fully bonded ground state (gel) network. We also find a confirmation of the results for the N_{max} model of a logarithmic dependence of S_{conf} on the energy, differently from the Gaussian behavior reported for fragile glass-formers. Hence, our work provides another example in favor of the analogy between gels and strong glass-formers. The study of the dynamical behavior of the density correlators and their wave-vector dependence, also in comparison with MCT predictions, will be the subject of future studies.

Acknowledgments

References

[1] Mezzenga R, Schurtenberger P, Burbidge A and Michel M 2005 *Nat. Mater.* **4** 729–40
[2] Sear R P 2006 *Curr. Opin. Colloid Interface Sci.* **11** 35
[3] Trappe V and Sandkühler P 2004 *Curr. Opin. Colloid Interface Sci.* **8** 494–500
[4] Cipelletti L and Ramos L 2005 *J. Phys.: Condens. Matter* **17** 253
[5] Sciortino F and Tartaglia P 2005 *Adv. Phys.* **54** 471–524
[6] Voigtmann T and Poon W C K 2006 *J. Phys.: Condens. Matter* **18** L465–9
[7] Zaccarelli E 2007 *J. Phys.: Condens. Matter* **19** 323101
[8] Pusey P N and van Megen W 1987 *Phys. Rev. Lett.* **59** 2083–6
[9] Zaccarelli E, Valeriani C, Sanz E, Poon W C K, Cates M E and Pusey P N 2009 *Phys. Rev. Lett.* **103** 135704
[10] Fabbian L, Götze W, Sciortino F, Tartaglia P and Thiery F 1999 *Phys. Rev. E* **59** 1347–50
[11] Bergenholtz J and Fuchs M 1999 *Phys. Rev. E* **59** 5706–15
[12] Dawson K A, Foffi G, Fuchs M, Götze W, Sciortino F, Sperl M, Tartaglia P, Voigtmann T and Zaccarelli E 2001 *Phys. Rev. E* **63** 011401
[13] Zaccarelli E, Foffi G, Dawson K A, Sciortino F and Tartaglia P 2001 *Phys. Rev. E* **63** 031501
[14] Puertas A M, Fuchs M and Cates M E 2002 *Phys. Rev. Lett.* **88** 098301
[15] Puertas A, Fuchs M and Cates M E 2003 *Phys. Rev. E* **67** 031406
[16] Zaccarelli E, Foffi G, Dawson K A, Buldrey S V, Sciortino F and Tartaglia P 2002 *Phys. Rev. E* **66** 041402
[17] Sciortino F, Tartaglia P and Zaccarelli E 2003 *Phys. Rev. Lett.* **91** 1–4
[18] Zaccarelli E, Löwen H, Wessels P P F, Sciortino F, Tartaglia P and Likos C N 2004 *Phys. Rev. Lett.* **92** 225703
[19] Eckert T and Bartsch E 2002 *Phys. Rev. Lett.* **89** 125701
[20] Pham K N, Puertas A M, Bergenholtz J, Egelhaaf S U, Moussaïd A, Pusey P N, Schofield A B, Cates M E, Fuchs M and Poon W C K 2002 *Science* **296** 104–6
[21] Pham K N, Egelhaaf S U, Pusey P N and Poon W C K 2004 *Phys. Rev. E* **69** 1–13
[22] Lu P J, Zaccarelli E, Ciulla F, Schofield A B, Sciortino F and Weitz D A 2008 *Nature* **453** 499–503
[23] Sastry S 2000 *Phys. Rev. Lett.* **85** 590–3
[24] Zaccarelli E, Buldyrev S V, La Nave E, Moreno A J, Saika-Voivod I, Sciortino F and Tartaglia P 2005 *Phys. Rev. Lett.* **94** 218301
[25] Bianchi E, Largo J, Tartaglia P, Zaccarelli E and Sciortino F 2006 *Phys. Rev. Lett.* **97** 168301
[26] Sciortino F, Buldyrev S, De Michele C, Ghofraniha N, La Nave E, Moreno A, Mossa S, Tartaglia P and Zaccarelli E 2005 *Comput. Phys. Commun.* **169** 166–71
[27] Fantoni R, Gazzillo D, Giacometti A, Miller M A and Pastore G 2007 *J. Chem. Phys.* **127** 234507
[28] Bianchi E, Tartaglia P, Zaccarelli E and Sciortino F 2008 *J. Chem. Phys.* **128** 144502
[29] Krzakala F, Tarzia M and Zdeborová L 2008 *Phys. Rev. Lett.* **101** 165702
[30] Gazzillo D, Fantoni R and Giacometti A 2008 *Phys. Rev. E* **78** 021201
[31] Giacometti A, Lado F, Largo J, Pastore G and Sciortino F 2009 *J. Chem. Phys.* **131** 174114
[32] Mirkin C A, Letsinger R L, Mucic R C and Storhoff J J 1996 *Nature* **382** 607–9
[33] Manoharan V N, Elsesser M T and Pine D J 2003 *Science* **301** 483–7
[34] Geerts N and Eiser E 2009 arXiv:0906.3137
[35] Glotzer S C and Solomon M J 2007 *Nat. Mater.* **6** 557–62
[36] Sciortino F 2008 *Eur. Phys. J.* B **64** 505–9
[37] Moreno A J, Buldyrev S V, La Nave E, Saika-Voivod I, Sciortino F, Tartaglia P and Zaccarelli E 2005 *Phys. Rev. Lett.* **95** 157802
[38] Zaccarelli E, Saika-Voivod I, Moreno A J, Buldyrev S V, Tartaglia P and Sciortino F 2006 *J. Chem. Phys.* **124** 124908
[39] De Michele C, Gabrielli S, Tartaglia P and Sciortino F 2006 *J. Phys. Chem.* B **110** 8064
[40] Starr F W and Sciortino F 2006 *J. Phys.: Condens. Matter* **18** L347–53
[41] Angell C A 1985 *J. Non-Cryst. Solids* **73** 1
[42] Stillinger F H and Weber T A 1982 *Phys. Rev. A* **25** 978–89

[43] Saika-Voivod I, Poole P H and Sciortino F 2001 *Nature* **412** 514–7

[44] Kauzmann W 1948 *Chem. Rev.* **43** 219

[45] Speedy R J and Debenedetti P G 1994 *Mol. Phys.* **81** 237

[46] Speedy R J and Debenedetti P G 1996 *Mol. Phys.* **88** 1293

[47] Zaccarelli E, Sciortino F and Tartaglia P 2007 *J. Chem. Phys.* **127** 174501

[48] Ferrante A and Tosi M P 1989 *J. Phys.: Condens. Matter* **1** 1679–94

[49] De Michele C, Tartaglia P and Sciortino F 2006 *J. Chem. Phys.* **125** 4710

[50] Foffi G, Dawson K A, Buldrey S V, Sciortino F, Zaccarelli E and Tartaglia P 2002 *Phys. Rev.* E **65** 050802

[51] Foffi G, Sciortino F, Tartaglia P, Zaccarelli E, Lo Verso F, Reatto L, Dawson K A and Likos C N 2003 *Phys. Rev. Lett.* **90** 238301

[52] Kumar P, Buldyrev S V, Sciortino F, Zaccarelli E and Stanley H E 2005 *Phys. Rev.* E **72** 021501

[53] Mayer C, Zaccarelli E, Stiakakis E, Likos C N, Sciortino F, Munam A, Gauthier M, Hadjichristidis N, Iatrou H, Tartaglia P, Löwen H and Vlassopoulos D 2008 *Nat. Mater.* **7** 780

[54] Del Gado E and Kob W 2005 *Europhys. Lett.* **72** 1032–8

[55] Toledano J, Sciortino F and Zaccarelli E 2009 *Soft Matter* **5** 2571

[56] Eckert T and Bartsch E 2003 *Faraday Discuss.* **123** 51–64

[57] Sperl M 2003 *Phys. Rev.* E **68** 031405

[58] Zaccarelli E, Foffi G, Sciortino F and Tartaglia P 2003 *Phys. Rev. Lett.* **91** 108301

[59] Zaccarelli E and Poon W C K 2009 *Proc. Natl Acad. Sci.* **106** 15203–8

[60] Largo J, Starr F W and Sciortino F 2007 *Langmuir* **23** 5896

[61] Sciortino F 2005 *J. Stat. Mech.* **5** 15

[62] Heuer A 2008 *J. Phys.: Condens. Matter* **20** K3101

[63] Moreno A J, Saika-Voivod I, Zaccarelli E, La Nave E, Buldyrev S V, Tartaglia P and Sciortino F 2006 *J. Chem. Phys.* **124** 204509

[64] Foffi G and Sciortino F 2006 *Phys. Rev.* E **74** 050401

[65] Frenkel D and Ladd A J C 1984 *J. Chem. Phys.* **81** 3188–93

[66] Sciortino F, Kob W and Tartaglia P 2000 *J. Phys.: Condens. Matter* **12** 6525–34

[67] Büchner S and Heuer A 1999 *Phys. Rev.* E **60** 6507–18

[68] Sastry S 2001 *Nature* **409** 164–7

[69] Adam G and Gibbs J H 1965 *J. Chem. Phys.* **43** 139

[70] Yuao X and Cormack A N 2002 *Comput. Mater. Sci.* **24** 343–60

[71] Coslovich D and Pastore G 2009 *J. Phys.: Condens. Matter* **21** 285107